Letter

Anomalous Hall metal and fractional Chern insulator in twisted transition metal dichalcogenides

Valentin Crépel [1,2] and Liang Fu [1]

[1] *Department of Physics, Massachusetts Institute of Technology, Cambridge, Massachusetts 02139, USA*

[2] *Center for Computational Quantum Physics, Flatiron Institute, New York, New York 10010, USA*

(Received 21 July 2022; revised 20 April 2023; accepted 1 May 2023; published 10 May 2023)

We predict robust Ising ferromagnetism driven by Coulomb interaction in the metallic phase of twisted transition metal dichalcogenide homobilayers for a range of small twist angles. Due to the presence of spin-valley locking and a Chern band, the completely spin-polarized state—a half metal—has a spin gap and exhibits the anomalous Hall effect. We also find that near a magic angle where the Chern band is predicted to be exceptionally flat, the anomalous Hall metal at 1/3 filling may become unstable at low temperature and change into a $\sqrt{3} \times \sqrt{3}$ charge density wave or a fractional Chern insulator.

DOI: 10.1103/PhysRevB.107.L201109

Introduction. Moiré materials based on two-dimensional (2D) van der Waals heterostructures have swiftly become an exciting platform for the realization of strongly correlated and topological electronic phases. Among these artificial quantum materials, a particular class—semiconductor transition metal dichalcogenide (TMD) heterobilayers—has recently attracted great interest and intensive study due to a plethora of novel electronic phases discovered therein, including Mott-Hubbard and charge-transfer insulators [1–4], generalized Wigner crystals [4–7], and the quantum anomalous Hall (QAH) state [8].

Another 2D-semiconductor-based platform to search for correlated topological phases is twisted TMD homobilayers (tTMDs). It was predicted early on [9] that due to spin-valley locking and spatially modulated interlayer tunneling, tTMDs host topological moiré bands of the Kane-Mele type [10] over a continuum of twist angles θ. They would lead to a quantum spin Hall state at the filling of $n = 2$ holes per moiré unit cell, which corresponds to the complete filling of the topmost moiré valence bands including both K and $-K$ valleys. Even more interesting is the possibility that at half band filling $n = 1$, electron interaction drives tTMDs into a completely valley-polarized state at zero external magnetic field, which would give rise to the QAH effect.

Experiments on twisted WSe_2 homobilayers ($tWSe_2$) at twist angles $\theta \sim 5^\circ$ have found an interaction-induced insulating state at $n = 1$ [11,12]. However, there is no spontaneous Hall effect at zero field, indicating the absence of valley polarization. This is likely due to the relatively large moiré bandwidth at the twist angles experimentally studied so far. To reduce the kinetic energy cost, an intervalley coherent state—which nullifies the Berry curvature by hybridizing opposite valleys—is found to be energetically favorable compared with the valley-polarized state [13–15].

A new opportunity opened up when recent theoretical modeling and large-scale density functional theory (DFT) calculations [16] found that the topological bands in $tWSe_2$ become extremely flat near a "magic angle" $\theta^* \simeq 1.45^\circ$. Such topological flat bands overcome the previous limitation and make this system a promising candidate for realizing interaction-induced topological phases. Indeed, Hartree-Fock calculations found the QAH insulator at $n = 1$ near this magic angle [16], which arises from spontaneous complete spin-valley polarization.

In this Research Letter, we use a variety of numerical methods to study interaction-induced electronic phases in tTMDs at $n < 1$ fillings of the flat band. We find robust Ising ferromagnetism in the metallic state over a range of fillings and twist angles. The spin-valley polarization is driven by Coulomb repulsion in the topological flat band. The completely polarized state extends up to relatively high temperature and to twist angle $\theta \sim 2.5^\circ$, a realistic regime for experiments.

We also show that a spontaneous fractional Chern insulator (FCI), also known as a fractional quantum anomalous Hall (FQAH) state, may be realized under suitable conditions at $n = 1/3$ filling of $tWSe_2$ near the magic angle. Importantly, the energy scale for an FQAH state at $n = 1/3$ is much smaller than the spin gap in most of the filling factor range $n \leqslant 1$. Our work highlights that Ising ferromagnetism leading to an anomalous Hall metal is a prerequisite to the highly sought-after FQAH state in tTMDs, which was also recently predicted in twisted bilayer $MoTe_2$ [17]. Our work also shows the stringent requirements for its realization, namely, the necessity of a magic angle and metallic gate to properly screen the Coulomb interaction, which may otherwise favor a competing charge density wave.

Generalized Kane-Mele model in tTMDs. We study two WSe_2 layers twisted by a small angle θ with respect to the AA stacking. The resulting moiré pattern forms a honeycomb lattice with XM and MX sites, where the chalcogen atom $X = Se$ on the top layer is aligned with the transition metal atom $M = W$ on the bottom layer, or vice versa [see inset in Fig. 1(b)]. The XM and MX sites are related by a twofold rotation symmetry interchanging the two layers.

The first and second moiré valence bands can thus be captured by an effective tight-binding model on the honeycomb lattice, originally introduced by Wu *et al.* [9]. Since the Wannier orbital on the XM (MX) site resides primarily on the top (bottom) layer, the nearest-neighbor hopping between different-sublattice sites is induced by interlayer

 ©2023 American Physical Society

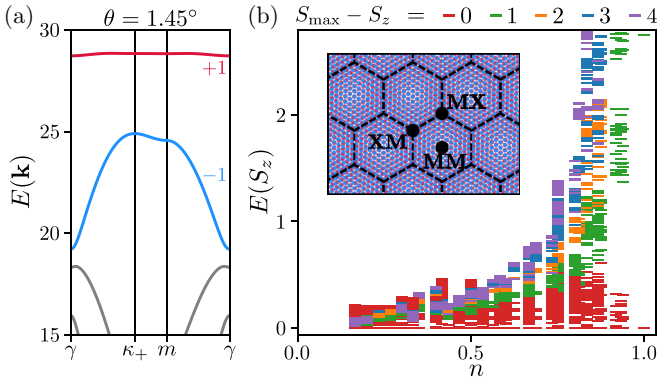

FIG. 1. (a) K valley moiré bands for a twisted WSe_2 homobilayer near the magic angle ($\theta = 1.45°$), with colors indicating their Chern numbers. The $-K$ valleys bands are time reversal conjugate and carry opposite Chern number. (b) All low-lying states of the interacting tight-binding model on the MX-XM honeycomb lattice (inset) are fully spin-valley polarized for densities $n \gtrsim 0.2$, as shown here for $U = 25$ meV $\gg w$. Only the lowest-lying eigenstates obtained by ED are displayed in each sector, their color corresponding to the total spin. The results for several lattice sizes (4×3, 4×4, 5×3, 5×4, and 6×5) with at least five particles are overlaid. Energies are given in meV and measured with respect to the ferromagnetic ground state.

tunneling, while second-nearest-neighbor hopping between same-sublattice sites arises from the moiré potential within each layer. Due to the twist angle, the $\pm K$ valley band edges of the top and bottom layers are displaced from each other in $\mathbf{k}$ space and located at the two corners of the mini Brillouin zone $\kappa_\pm$. As a result, the second-neighbor hopping t_2 in the effective tight-binding model acquires a phase factor $e^{\pm i\phi}$ with $\phi \sim \boldsymbol{K} \cdot \boldsymbol{a}_M = 2\pi/3$ ($\boldsymbol{a}_M$ is a primitive moiré lattice vector), which is opposite for the $\pm K$ valley. Due to spin-valley locking in the WSe_2 monolayers, the $\pm K$ valleys also correspond to opposite spins $s_z = \uparrow, \downarrow$.

The resulting model is therefore a generalization of the Kane-Mele model:

$$\mathcal{H} = \sum_n \sum_{\langle \boldsymbol{r}, \boldsymbol{r}' \rangle_n} (t_n c^\dagger_{\boldsymbol{r},\uparrow} c_{\boldsymbol{r}',\uparrow} + t_n^* c^\dagger_{\boldsymbol{r},\downarrow} c_{\boldsymbol{r}',\downarrow} + \text{H.c.}) + V_n n_{\boldsymbol{r}} n_{\boldsymbol{r}'}. \quad (1)$$

Here, the c's are fermionic operators for holes, while $\langle \boldsymbol{r}, \boldsymbol{r}' \rangle_n$ denotes hopping between nth neighbors on the honeycomb lattice. Importantly, long-range hoppings $t_{n=1,\ldots,5}$ are included to faithfully reproduce the *ab initio* band structure determined by large-scale DFT [18]. Amongst these tunneling amplitudes, only t_2 has an appreciable imaginary component consistent with $\phi \sim 2\pi/3$. As a result, the first and second moiré valence bands are separated by a topological gap and carry a spin Chern number $C_s^1 = 1$ and $C_s^2 = -1$, respectively, where $C_s \equiv C_\uparrow = -C_\downarrow$ follows from time-reversal symmetry [see Fig. 1(a)].

Of prime importance to our work is the θ-dependent bandwidth of the topmost valence band [18], which exhibits a deep minimum near a magic angle of $\theta^* \simeq 1.45°$ where it reaches values $w \sim 60$ μeV [see Fig. 1(a)]. The presence of topological flat bands makes tTMDs susceptible to interaction-driven spin-valley polarization. In the following analysis, we shall first consider only on-site repulsion, i.e., $V_0{=}U$ and $V_{n\geqslant 1}{=}0$. This simplification captures the dominant part of the Coulomb potential for the small twist angles considered here and can also be experimentally realized via gate screening, as shown in recent experiments on TMD heterostructures [19–22].

Half metal. By exact diagonalization (ED) of Eq. (1) with on-site repulsion U, we find Ising ferromagnetism with complete spin-valley polarization in a wide range of fillings $0.2 < n \leqslant 1$ around the magic angle. The fully polarized ground state below unit filling is obtained by occupying the lowest-energy orbitals of the topmost moiré band of one spin (= valley) component only, therefore avoiding U completely. The resulting state is a ferromagnetic metal, also known as a half metal.

Figure 1(b) shows the low-lying energy states at θ^*, including several spin flips ($S_{\max} - S_z = 0, \ldots, 4$) above the fully spin-↑-polarized sector. While we fix $U = 25$ meV, the precise value of the on-site repulsion does not matter as long as it largely exceeds all energy scales involved in the tight-biding model. Our results for various system sizes indicate a spin gap for $n \gtrsim 0.2$. Moreover, a manifold of fully polarized many-body states is present at energies below the spin gap, corresponding to particle-hole excitations around the Fermi surface.

The presence of a spin gap in the fully polarized metal (as opposed to gapless magnons) is made possible by the strong spin-orbit coupling in TMDs, which reduces the SU(2) spin symmetry to U(1). Our ED study shows that the lowest-energy spin excitation corresponds to a single spin flip; hence the spin gap is given by $\Delta_{\text{SG}} = E(S_{\max} - 1) - E(S_{\max})$. A physical picture for the spin gap in $t\text{WSe}_2$ is that a spin-↓ fermion cannot completely avoid overlap with all spin-↑ fermions and completely avoid kinetic energy cost.

A necessary condition for spontaneous and complete spin-valley polarization is $\Delta_{\text{SG}} > 0$. By calculating Δ_{SG} with a spin-flip analysis (see Supplemental Material [18]), we identify the region of half metal as a function of filling factor and twist angle $\theta < 1.5°$, shown in Fig. 2. Large values of the gap indicate Ising ferromagnetism persisting at higher temperatures, which is found near unit filling $n = 1$ and close to the magic angle θ^*.

For $\theta > 1.5°$, the first and second moiré valence bands carry identical spin Chern numbers $C_s^1 = C_s^2$, which cannot be captured by the two-band model equation (1). To extend our analysis to larger twist angles, we study the continuum model of WSe_2 homobilayers [9,16] with electron interaction. The spin-flip analysis can be applied to the continuum if the gate-screened Coulomb interaction is approximated by a contact repulsion [23]. Despite being a crude approximation, it nevertheless reproduces essential features of our lattice model result [18] and can therefore be used as a qualitative guide to the half metal.

The spin-flip results for the interacting continuum model are shown in Fig. 2 for $\theta > 1.5°$, where we observe that the half metal extends up to $\theta \sim 2.5°$ and in a wide range of densities. The spin gap reaches maximal values of ∼3.5 meV, which suggests a ferromagnetic critical temperature T_{FM} on the order of 40 K. We also observe that the spin gap is maximum for densities below unit filling when $\theta > 1.75°$, indicating that the half metal can be more robust than the QAH insulator at $n = 1$. We finally notice that the spin gap

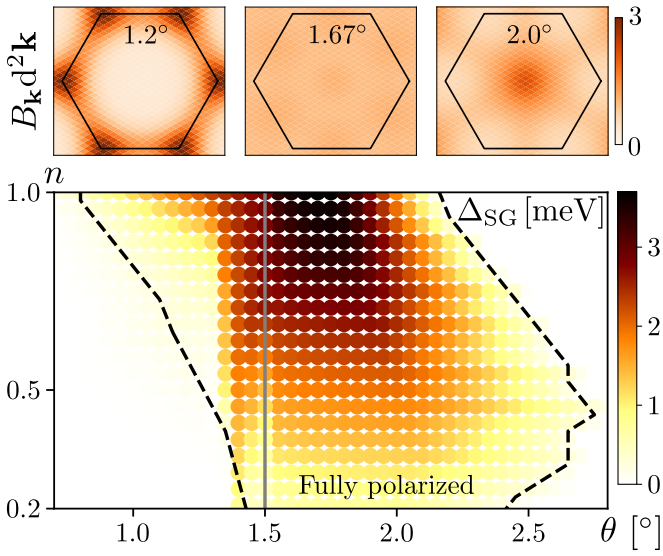

FIG. 2. Spin gap Δ_{SP} obtained from a spin-flip analysis on the tight-binding ($\theta < 1.5°$) and continuum ($\theta > 1.5°$) models with 576 points in the moiré Brillouin zone. The dashed line encircles the region in which the system is fully spin-valley polarized. The spin gap is largest where the Berry curvature's fluctuations are minimal (panels at top), showing a close connection between ferromagnetism and topology.

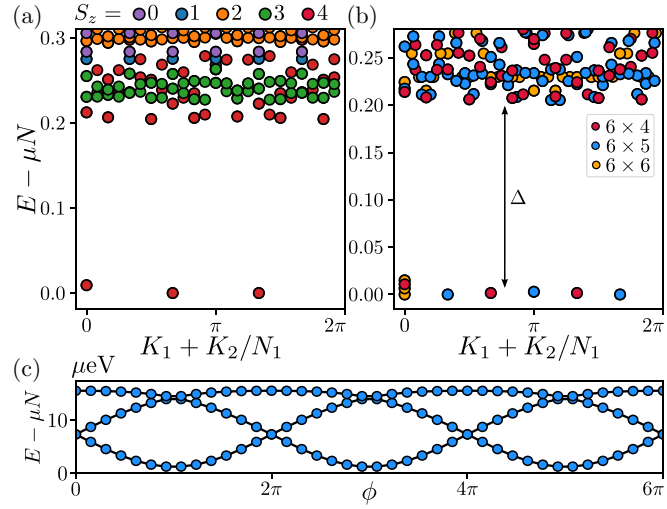

FIG. 3. (a) Many-body spectrum at filling $n = 1/3$ as a function of the many-body momentum (K_1, K_2) for $V = 3.5$ meV and $\theta = 1.4°$, obtained with ED on a 6×4 lattice including all spin sectors. Energies are given in meV. The system remains fully spin-valley polarized. (b) Same as (a) in the fully spin-polarized sector and for larger system sizes. Three low-lying states clearly detach from the continuum. (c) Their spectral flow exhibits the characteristic 6π periodicity of FCI ground states. In all plots, μ is a chemical potential used to overlay the various system sizes.

qualitatively correlates with the variance of the Berry curvature (panels at top of Fig. 2), suggesting an intimate relation between topology and Ising ferromagnetism in our model.

To summarize the first part of this work, we predict a robust half-metallic phase in twisted WSe_2 in the experimentally accessible regime $\theta < 2.5°$ and $n < 1$. This phase is stabilized by the short-ranged and dominant part of the Coulomb repulsion, which enables a relatively high ferromagnetic temperature that can reach a few tens of kelvins. Thanks to the spin-valley locking in TMDs, the Ising ferromagnetism can be detected optically through circular dichroism. The presence of Berry curvature and band topology is manifested by the anomalous Hall effect in the half metal.

The on-site repulsion U is crucial in inducing complete spin-valley polarization with a spin gap but has no effects in the fully spin-valley-polarized phase. As a result, below T_{FM}, the subdominant components of the interactions $V_{n\geqslant 1}$, up to now neglected, may have an important effect in determining the ground state of the system. If $V_{n\geqslant 1}$ are small compared with the spin gap, the low-temperature phase will remain fully polarized. Therefore, thanks to the hierarchy in energy scales between the short- and long-range parts of the Coulomb repulsion on the moiré lattice, the half metal that has its onset at high temperature is a precursor to and a parent state of low-temperature phases in $tWSe_2$, which we now turn to.

Fractional quantum anomalous Hall insulator. We now show via a comprehensive ED study that a spontaneous fractional Chern insulator, also known as a fractional quantum anomalous Hall (FQAH) state, may arise in a twisted WSe_2 homobilayer. Its appearance follows the general argument given above: (i) The system at fractional filling $n = 1/3$ shows spontaneous complete spin-valley polarization around θ^* with a spin gap of 0.13 meV (see Fig. 2); (ii) in the fully polarized phase, the generalized Kane-Mele model equation (1) reduces to a Haldane model with long-range hoppings [24], for which consistent evidence from ED [25–27] and the density-matrix renormalization group (DMRG) approach [28] has shown the emergence of a fractional Chern insulator.

To put these ideas on firm ground, we first consider $V_1 = V = 3.5$ meV and $V_{n>1} = 0$, keeping $U = 25$ meV as before, and perform extensive ED calculations to find the ground state of Eq. (1) projected to the first moiré band [29–32]. We perform calculations on finite clusters with $N_1 \times N_2$ unit cells along the two moiré lattice basis vectors, with a total number of holes equal to $N = N_\uparrow + N_\downarrow = N_1 N_2/3$. Translation invariance allows us to resolve the many-body momenta (K_1, K_2) along the two moiré basis vectors.

For consistency, we first check that the system is fully spin-valley polarized. Our ED results at the magic angle on the 6×4 lattice including all spin sectors, shown in Fig. 3(a), prove that the model at filling $n = 1/3$ is indeed ferromagnetic. The energy of a single spin flip extracted from these data, $\Delta_{\mathrm{SG}} \simeq 0.15$ meV, almost quantitatively matches the value obtained in Fig. 2 for $n = 1/3$ at $V = 0$ and $\theta = 1.45°$.

We also notice three low-lying and almost degenerate states, which are clearly detached from the many-body continuum and appear for all considered system sizes $6 \times N_2$ with $N_2 = 4, 5, 6$ [Fig. 3(b)]. They are located at many-body momenta $K_1 = \frac{2\pi}{3}[0, N_2, 2N_2] + Q_1$ and $K_2 = 0$, with a Jordan-Wigner shift $Q_1 = 0$ if N_2 is even and $Q_1 = \pi/6$ if it is odd, which precisely match the counting rule of a Laughlin-like FCI [27,29,33]. As another piece of evidence of the FCI behavior, we compute the anomalous Hall conductance associated with the ground-state manifold $\sigma = \frac{e^2}{h}\frac{2\pi}{N_1 N_2}\sum_{\boldsymbol{k}} n_{\boldsymbol{k}} B_{\boldsymbol{k}}$, with $n_{\boldsymbol{k}}$ being the mean occupation of the $\boldsymbol{k}$ single-particle

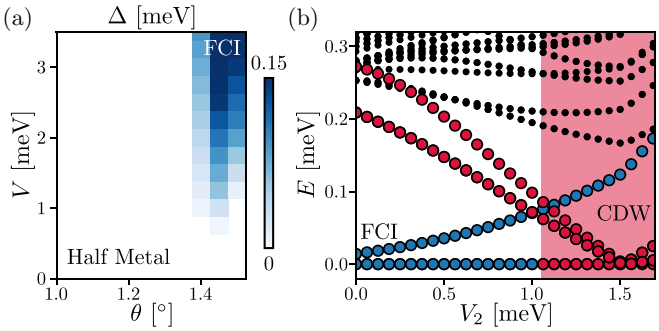

FIG. 4. (a) FQAH many-body gap as a function of interaction strength V and twist angle θ. The half metal dominates the phase diagram except near the magic angle, where FCI behaviors emerge. (b) Longer-range interaction drives a transition from the FQAH state to a CDW state. For visibility, we have colored the state connected to the FCI (CDW) in blue (red).

state in the three nearly degenerate ground states and $B_{\boldsymbol{k}}$ being the single-particle Berry curvature [34,35]. In units of $e^2C_s^1/h$, we find $\sigma_{xy} = 0.33$, 0.32, and 0.31 for $N_2 \in \{4, 5, 6\}$ [36], in excellent agreement with the theoretical expectation of $\sigma_{xy}^{\mathrm{FCI}} = 1/3$.

Finally, a necessary condition for the emergence of the FCI—which is also sufficient if the gap Δ does not close in the thermodynamic limit [29,37,38]—is that each topological ground state must undergo cyclic permutation when ϕ goes from 0 to 2π such that it comes back only after three units of flux ($\phi = 6\pi$) [39]. As shown in Fig. 3(c) for the 6×5 lattice, this necessary condition is satisfied in our model. Altogether, the numerical evidence presented in Figs. 3(a)–3(c) (additional evidence is provided in the Supplemental Material [18]) clearly identifies an FQAH phase at fractional filling of our tTMDs, with a spontaneous spin-valley polarization inherited from the parent half metal. A similar FQAH state was found in $t\mathrm{MoTe}_2$ [17].

To further probe the robustness of the FQAH phase, we compute the many-body gap Δ above its ground-state manifold (defined in Fig. 3) as a function of interaction strength and twist angle. Our results presented in Fig. 4(a) are consistent with our previous findings; near the magic angle, the half metal found at $V = 0$ (Fig. 2) becomes unstable and changes into a FCI when V increases (Fig. 3). The situation quickly becomes unfavorable for the FQAH state as one moves away from the magic angle, with Δ almost halved when θ goes away from the magic angle by $\delta\theta = 0.05^\circ$. Even worse, for deviations $\theta \sim 0.15^\circ$, the complete spin-valley ferromagnetism is lost as the spin gap at $n = 1/3$ closes near $\theta = 1.3^\circ$ (Fig. 1). The observation of an FQAH state in $t\mathrm{WSe}_2$ thus requires stringent experimental conditions and, in particular, accurate control of the twist angle.

Another perturbation reducing the FQAH many-body gap comes from the longer-range part of the interaction $V_{n>1}$. Indeed, the ground state at filling $n = 1/3$ when $V_1 = V_2 = \infty$ is a charge density wave (CDW) of $\sqrt{3} \times \sqrt{3}$ periodicity [40]. An FQAH-to-CDW transition is thus expected as V_2 increases. Because such a CDW only occupies one of the honeycomb sublattices, band-projected ED cannot faithfully describe it as the topmost valence band is sublattice hybridized. To resolve this issue, we perform ED in real space using a 6×4 lattice. To keep the Hilbert space manageable, we discard any configuration with a nonzero number of double occupation or nearest-neighbor pair [28,41].

The results of this analysis, depicted in Fig. 4(b), show a transition from a threefold to a sixfold degenerate ground state as V_2 increases [42]. The former satisfies the Laughlin-like counting rule and represents the previously identified FQAH state, while the degeneracy of the latter perfectly matches the expectation for a CDW on the honeycomb lattice. We find that the transition between the FQAH state and the CDW state occurs around $V_2^c \simeq 1.05$ meV. For $V_1 = 3.5$ meV, this corresponds to $V_1 \simeq 1.8\sqrt{3}V_2^c$. Therefore the realization of the FQAH state requires screening from nearby metallic gates to decrease the V_1/V_2 ratio by a factor of at least 2 compared with its Coulomb value. The competition between FQAH and CDW states and the importance of gate screening have been overlooked in previous studies on tTMDs.

Our FQAH state with spontaneous spin-valley polarization at zero field should be contrasted with the FCIs reported in graphene/hexagonal boron nitride (hBN) and magic-angle twisted bilayer graphene, which rely on sufficiently large external magnetic fields. For instance, the most recent experiment on magic-angle graphene [43] finds an incompressible state with *zero* Hall conductance for magnetic fields below 5 T at $3 + 1/3$ filling of the flat band, while the evidence for FCIs—fractional slope and fractional intercept of incompressible states—shows up at higher field. As an alternative scenario, however, the observed feature could also arise if a CDW at 1/3 filling of a trivial flat band coexists with a $\nu = 1/3$ fractional quantum Hall state from Landau levels of a dispersive band. The search for the anomalous Hall effect [44] and FQAH state in twisted bilayer graphene at fractional fillings [45–51] continues.

Our work highlights the importance of the anomalous Hall metal state as a precursor to the FQAH state in TMD moiré heterostructures having topological flat bands. While our calculations were performed for $t\mathrm{WSe}_2$, our main conclusion also applies to other twisted TMD homobilayers, although the magic angle and the maximum spin gap are material dependent.

Acknowledgments. We are grateful to Trithep Devakul and Yang Zhang for a previous collaboration that motivated and paved the way for this study. Our work is supported by the Simons Foundation through a Simons Investigator award. L.F. is partly supported by the David and Lucile Packard Foundation. V.C. gratefully acknowledges support from the MathWorks fellowship.

[1] F. Wu, T. Lovorn, E. Tutuc, and A. H. MacDonald, Phys. Rev. Lett. **121**, 026402 (2018).

[2] Y. Zhang, N. F. Q. Yuan, and L. Fu, Phys. Rev. B **102**, 201115(R) (2020).

[3] Y. Tang, L. Li, T. Li, Y. Xu, S. Liu, K. Barmak, K. Watanabe, T. Taniguchi, A. H. MacDonald, J. Shan, and K. F. Mak, Nature (London) **579**, 353 (2020).

[4] E. C. Regan, D. Wang, C. Jin, M. I. B. Utama, B. Gao, X. Wei, S. Zhao, W. Zhao, Z. Zhang, K. Yumigeta, M. Blei, J. D. Carlström, K. Watanabe, T. Taniguchi, S. Tongay, M. Crommie, A. Zettl, and F. Wang, Nature (London) **579**, 359 (2020).

[5] Y. Xu, S. Liu, D. A. Rhodes, K. Watanabe, T. Taniguchi, J. Hone, V. Elser, K. F. Mak, and J. Shan, Nature (London) **587**, 214 (2020).

[6] X. Huang, T. Wang, S. Miao, C. Wang, Z. Li, Z. Lian, T. Taniguchi, K. Watanabe, S. Okamoto, D. Xiao, S.-F. Shi, and Y.-T. Cui, Nat. Phys. **17**, 715 (2021).

[7] H. Li, S. Li, E. C. Regan, D. Wang, W. Zhao, S. Kahn, K. Yumigeta, M. Blei, T. Taniguchi, K. Watanabe, S. Tongay, A. Zettl, M. F. Crommie, and F. Wang, Nature (London) **597**, 650 (2021).

[8] T. Li, S. Jiang, B. Shen, Y. Zhang, L. Li, Z. Tao, T. Devakul, K. Watanabe, T. Taniguchi, L. Fu, J. Shan, and K. F. Mak, Nature (London) **600**, 641 (2021).

[9] F. Wu, T. Lovorn, E. Tutuc, I. Martin, and A. H. MacDonald, Phys. Rev. Lett. **122**, 086402 (2019).

[10] C. L. Kane and E. J. Mele, Phys. Rev. Lett. **95**, 226801 (2005).

[11] L. Wang, E.-M. Shih, A. Ghiotto, L. Xian, D. A. Rhodes, C. Tan, M. Claassen, D. M. Kennes, Y. Bai, B. Kim, K. Watanabe, T. Taniguchi, X. Zhu, J. Hone, A. Rubio, A. N. Pasupathy, and C. R. Dean, Nat. Mater. **19**, 861 (2020).

[12] A. Ghiotto, E.-M. Shih, G. S. Pereira, D. A. Rhodes, B. Kim, J. Zang, A. J. Millis, K. Watanabe, T. Taniguchi, J. C. Hone, L. Wang, C. R. Dean, and A. N. Pasupathy, Nature (London) **597**, 345 (2021).

[13] Z. Bi and L. Fu, Nat. Commun. **12**, 642 (2021).

[14] J. Zang, J. Wang, J. Cano, and A. J. Millis, Phys. Rev. B **104**, 075150 (2021).

[15] J. Zang, J. Wang, J. Cano, A. Georges, and A. J. Millis, Phys. Rev. X **12**, 021064 (2022).

[16] T. Devakul, V. Crépel, Y. Zhang, and L. Fu, Nat. Commun. **12**, 6730 (2021).

[17] H. Li, U. Kumar, K. Sun, and S.-Z. Lin, Phys. Rev. Res. **3**, L032070 (2021).

[18] See Supplemental Material at http://link.aps.org/supplemental/10.1103/PhysRevB.107.L201109 for details.

[19] Z. Qiu, M. Trushin, H. Fang, I. Verzhbitskiy, S. Gao, E. Laksono, M. Yang, P. Lyu, J. Li, J. Su, M. Telychko, K. Watanabe, T. Taniguchi, J. Wu, A. H. Castro Neto, L. Yang, G. Eda, S. Adam, and J. Lu, Sci. Adv. **5**, eaaw2347 (2019).

[20] Z. A. H. Goodwin, F. Corsetti, A. A. Mostofi, and J. Lischner, Phys. Rev. B **100**, 121106(R) (2019).

[21] M. Kim, S. Xu, A. Berdyugin, A. Principi, S. Slizovskiy, N. Xin, P. Kumaravadivel, W. Kuang, M. Hamer, R. Krishna Kumar, R. V. Gorbachev, K. Watanabe, T. Taniguchi, I. V. Grigorieva, V. I. Fal'ko, M. Polini, and A. K. Geim, Nat. Commun. **11**, 2339 (2020); **11**, 3054(E) (2020).

[22] Y. Xu, K. Kang, K. Watanabe, T. Taniguchi, K. F. Mak, and J. Shan, Nat. Nanotechnol. **17**, 934 (2022).

[23] Y. Alavirad and J. Sau, Phys. Rev. B **102**, 235123 (2020).

[24] F. D. M. Haldane, Phys. Rev. Lett. **61**, 2015 (1988).

[25] Y.-L. Wu, B. A. Bernevig, and N. Regnault, Phys. Rev. B **85**, 075116 (2012).

[26] E. Dobardžić, M. V. Milovanović, and N. Regnault, Phys. Rev. B **88**, 115117 (2013).

[27] B. A. Bernevig and N. Regnault, Phys. Rev. B **85**, 075128 (2012).

[28] A. G. Grushin, J. Motruk, M. P. Zaletel, and F. Pollmann, Phys. Rev. B **91**, 035136 (2015).

[29] N. Regnault and B. A. Bernevig, Phys. Rev. X **1**, 021014 (2011).

[30] D. Sheng, Z.-C. Gu, K. Sun, and L. Sheng, Nat. Commun. **2**, 389 (2011).

[31] T. Neupert, L. Santos, C. Chamon, and C. Mudry, Phys. Rev. Lett. **106**, 236804 (2011).

[32] V. Crépel, B. Estienne, and N. Regnault, Phys. Rev. B **101**, 235158 (2020).

[33] V. Crépel, B. Estienne, B. A. Bernevig, P. Lecheminant, and N. Regnault, Phys. Rev. B **97**, 165136 (2018).

[34] A. G. Grushin, T. Neupert, C. Chamon, and C. Mudry, Phys. Rev. B **86**, 205125 (2012).

[35] T. Neupert, L. Santos, C. Chamon, and C. Mudry, Phys. Rev. B **86**, 165133 (2012).

[36] In this calculation, both the Berry curvature B_k and the Chern number $C_\uparrow$ were computed with the finite momentum discretization imposed by the $6 \times N_2$ lattice [52].

[37] V. Crépel, N. Regnault, and B. Estienne, Phys. Rev. B **100**, 125128 (2019).

[38] The many-body gap Δ appears robust in our calculations and even slightly increases with the number of particles (see Fig. 3). This is in sharp contrast with the FCI of the original Haldane model, i.e., without the longer-range hopping of Eq. (1) and with t_2 being purely imaginary, where the many-body gap suddenly drops on the 6×6 lattice due to commensuration effects stabilizing a CDW; see Refs. [25,28].

[39] D. J. Thouless, Phys. Rev. B **40**, 12034(R) (1989).

[40] Y. Zhang, T. Liu, and L. Fu, Phys. Rev. B **103**, 155142 (2021).

[41] S. Kourtis, T. Neupert, C. Chamon, and C. Mudry, Phys. Rev. Lett. **112**, 126806 (2014).

[42] The inversion symmetry of the model makes states at momenta (K_1, K_2) and $(-K_1, -K_2)$ coincide.

[43] Y. Xie, A. T. Pierce, J. M. Park, D. E. Parker, E. Khalaf, P. Ledwith, Y. Cao, S. H. Lee, S. Chen, P. R. Forrester, K. Watanabe, T. Taniguchi, A. Vishwanath, P. Jarillo-Herrero, and A. Yacoby, Nature (London) **600**, 439 (2021).

[44] M. Xie and A. H. MacDonald, Phys. Rev. Lett. **127**, 196401 (2021).

[45] P. J. Ledwith, G. Tarnopolsky, E. Khalaf, and A. Vishwanath, Phys. Rev. Res. **2**, 023237 (2020).

[46] C. Repellin and T. Senthil, Phys. Rev. Res. **2**, 023238 (2020).

[47] Z. Liu, A. Abouelkomsan, and E. J. Bergholtz, Phys. Rev. Lett. **126**, 026801 (2021).

[48] B. Andrews and A. Soluyanov, Phys. Rev. B **101**, 235312 (2020).

[49] A. Abouelkomsan, Z. Liu, and E. J. Bergholtz, Phys. Rev. Lett. **124**, 106803 (2020).

[50] D. Parker, P. Ledwith, E. Khalaf, T. Soejima, J. Hauschild, Y. Xie, A. Pierce, M. P. Zaletel, A. Yacoby, and A. Vishwanath, arXiv:2112.13837.

[51] P. Wilhelm, T. C. Lang, and A. M. Läuchli, Phys. Rev. B **103**, 125406 (2021).

[52] T. Fukui, Y. Hatsugai, and H. Suzuki, J. Phys. Soc. Jpn. **74**, 1674 (2005).